Photogrammetric digitisation of a bronze head – Surveying inside and outside for thickness measurement

Luca Perfetti [1], Giorgio Paolo Maria Vassena [1], Francesca Morandini [2], Francesco Fassi [3]

[1] Università degli Studi di Brescia, dept. of Civil Engineering, Architecture, Territory, Environment and Mathematics (DICATAM), Italy – (luca.perfetti; giorgio.vassena)@unibs.it
[2] Comune di Brescia, Fondazione Brescia Musei, Italy – morandini@bresciamusei.com
[3] Politecnico di Milano, dept. of Architecture, Built environment and Construction engineering (ABC), Italy – francesco.fassi@polimi.it

Keywords: Photogrammetry, Digitisation, Cross-polarisation, Fisheye, 3D asset, Cultural Heritage, thickness measurement

Abstract

This paper presents an effective and low-cost approach for the digitisation of a Roman bronze head exhibited at the Santa Giulia Museum in Brescia using close-range photogrammetry. The artefact posed significant challenges due to its dark, reflective exterior surface and its hollow interior, accessible only through an 8 cm neck opening. The digitisation had two main objectives: (1) to support restoration activities by accurately measuring the thickness of the bronze cast, and (2) to enhance the artefact's dissemination by producing a web-optimised digital replica.
Special emphasis was placed on the survey of the internal surface, achieved using a custom-designed camera probe equipped with a 5 megapixels RGB global shutter camera and LED ring lights. With this setup it was possible to effectively captured the inner geometry using low-cost tools. The internal dataset was connected with the exterior dataset, acquired by a regular DSLR and turntable setup supported by cross-polarization.
The processing workflow involved generating a high-resolution mesh model (~80M faces) and computing the cast's thickness using two methods: the M3C2 algorithm and the Shrinking Sphere algorithm, which provided consistent results. Additionally, an optimised low-poly version of the model was created for web sharing. This study highlights the potential of low-cost tailored photogrammetric solutions/workflows to address the complexities of digitising intricate museum artefacts.

1. Introduction

For the purpose of accurately digitising museal artefacts, among state-of-the-art digitisation techniques able to reconstruct the object shape and material texture, close-range photogrammetry is one that does not comprise a standardised acquisition procedure and whose effectiveness depends greatly on the capture design and overall carried out operations; ultimately, on the expertise of the photogrammetrists. In this context, many researchers have suggested protocols to streamline the photogrammetric acquisition (Menna et al., 2016; Marshall et al., 2019; Kalinowski et al., 2022) and prominent institutions have proposed advanced tools (Santos et al., 2014; Comte et al. 2024) aimed at optimizing the digitisation process, ultimately reducing the time required to acquire large quantities of assets. A notably example of such high-efficiency automated systems is CultLab3D developed by the Fraunhofer Institute for Computer Graphics Research IGD (Santos et al., 2014; Santos et al., 2017) which also feature a robotic arm designed to reach the undercuts and hard to reach areas of complex artefacts (CultArm3D). Nevertheless, the range of differences and variability of the multiple artefacts present in one museum alone in terms of shape, size, colour, reflectivity and material properties is such to hamper the realisation of one optimized tool/protocol that can fit all needs. As an example: the inner surface of hollow artefacts such as vases and hollow casts remain out of reach.
On the other hand, close-range photogrammetry offers just the required flexibility to fit most, if not all, needs of geometric digitisation. An ad-hoc acquisition design – limited to few artefacts – enables finding solutions to even the most complex digitisation challenges and, in this contest, even relatively low-cost tools can produce peak results.

In this paper we describe the photogrammetric acquisition designed ad-hoc and carried out for the digitisation of a 1:1 sized roman bronze head. The aim of the digitization was primarily to obtain the full 3D model of the artefact of both the outer surface and the hollow inside to enable the measurement of the thickness of the cast (Figure 1).

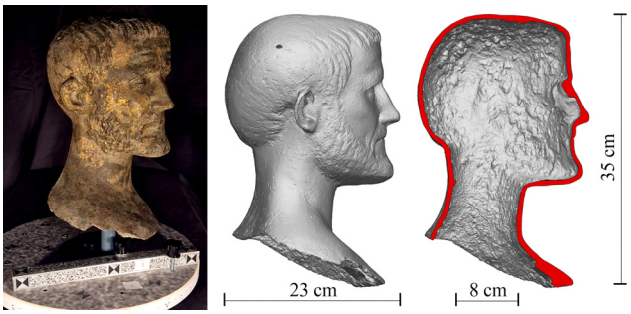

Figure 1. Bronze head artefact under investigation (Brini et al., In press): pictures of the head (left) and reconstructed 3D model with dimensions (right).

Bronze heads present significant challenges for the digitization process due to certain inherent characteristics that make the 3D acquisition complex and that requires dedicated solutions:

- **Hollow inside** – The inner surface of bronze heads can only be accessed through the narrow neck opening (Figure 1). Conducting a 3D survey in this confined space to measure the cast's thickness accurately is a demanding task. This challenge is particularly prohibitive for automated systems like CultLab3D (Santos et al., 2014) and methods, such as structured light scanners and handheld scanning systems that cannot fit the inside and

frame the undercuts (e.g., Artec3D inc., 2024; Creaform inc., 2024).

- **Dark colour / low albedo** – The bronze of ancient artefacts often exhibits a dark or greenish tint due to surface alterations. This material is generally characterized by a low albedo, which can limit the effectiveness of photogrammetry. As a result, bronze artefacts are regarded as some of the most challenging objects to digitize (Nicolae et al., 2014).
- **Specular reflections** – as added difficulty in the survey of bronze there is its reflectivity causing specular reflections (Nicolae et al., 2014; Bici et al., 2020), this phenomenon is further amplified for those bronze artefact that undergone gilding (Brini et al., In press). This is a strong limiting factor for photogrammetry constituting a challenge for the acquisition design.

From a photogrammetric point of view the survey of the outer surface pose some non-trivial challenges, Nevertheless, these challenges can be effectively addressed using consolidated methods and indeed also with relatively affordable acquisition solutions. High efficiency automated systems such as the CultLab3D (Santos et al., 2014) are very effective in digitizing the outer surface of bronze artefacts since they are capable of recording both the geometry of the object as well as its material properties. Regarding classical close-range photogrammetry with low-cost tools, a simple and efficient image acquisition network for the outer surface can be implemented using a DSLR (Digital Single Lens Reflex) and a classical turntable setup (Guidi et al., 2015; Menna et al., 2017; Lauria et al., 2022). Carrying out the acquisition under a controlled illumination setup allows overcoming both the issue of low albedo and that of specular reflections. The cross-polarization technique (Wells et al., 2005) effectively implemented in previous studies (Menna et al., 2016; Hallot and Gil, 2019; Mandelli et al., 2019; Adami et al., 2022) can be used to suppress the specular reflections of the gilded bronze.

The most challenging aspect in measuring the thickness of hollow artefacts, is surveying the inner surface. While Computed Tomography (CT) is the ideal technique in such cases (Bettuzzi et al., 2015; Albertin et al., 2019; Bossema et al., 2024), CT only provides the geometry of the artefact without capturing the material texture, which is important for conservation studies. Additionally, the complexity of operations, limited availability, and high cost of CT equipment make it less suitable in cases where Structure from Motion (SfM), can be employed. Therefore, the core challenge lies in ensuring that an image-based mapping device can: (1) enter the head through the neck opening, and (2) frame all intricate undercuts, such as those found in the nose and, most critically, the chin (Figure 1). General-purpose automated systems are not suitable for this specific task and, as a result, tailored solutions must be developed within an ad-hoc acquisition design framework. Potential image-based approaches involve the use of endoscopes, miniature cameras, compact spherical cameras, or small industrial cameras. Critical considerations for these solutions must include: (1) short focusing distance, devices must be capable of focusing at distances of less than 10 cm; (2) illumination, effective strategies are needed to adequately light the interior of the artefact; (3) camera mobility, systems must enable the camera to manoeuvre/rotate inside the artefact to capture undercuts all around.

1.1 Case study

The bronze head subject to this investigation is exhibited at the Santa Giulia Museum in Brescia. It is a male portrait from the 3rd century AD, perhaps of the emperor Probus, and part of a large group of Roman-era bronzes discovered in Brescia in the 19th century. The group of bronzes was discovered during an archaeological excavation campaign that began in 1823. The investigation, which started from an architectural element that emerged in the garden of a private property at the foot of the Cidneo Hill, brought to light the Flavian-era temple, including a large part of the original marble decorative elements and stone furnishings. On July 20, in 1826, between two of the main walls of the Capitoline temple, a deposit of bronze works was identified, consisting of more than three hundred pieces, mixed with soil, and burnt coals, including the renowned Winged Victory, one of the most important roman-era statues, also recently renovated (Patera & Morandini, 2021). The other bronzes found in the deposit include part of statues, frames likely belonging to the decoration of architecture or monuments such as inscriptions or bases, a gilded applique depicting a prisoner, functional elements of uncertain use, and finally, six heads. The chronological range of the pieces extends from the Julio-Claudian Era (mid-1st century AD to the 3rd century AD). The reason and date of this concealment are unknown.
Two male portraits, gilded and originally part of statues, currently appear very different; MR352 should probably be interpreted as emperor Aurelian (reign 270-275 AD) and MR353 as emperor Probus (reign 276-282 AD). This is because the work we are focusing on, MR353, has not yet undergone any specific interventions. Today, the Roman portraits are the subject of an interdisciplinary study project originating from the collaboration between the Museum of Brescia (run by the Municipality of Brescia and by the Brescia Museums Foundation) and the Opificio delle Pietre Dure in Florence on behalf of the Ministry of Culture (Brini, et al., In press).

MR353 (Figure 1) was cast using the lost-wax technique with the indirect method. The surface gilding, applied using the leaf technique, appears, as far as can be assessed at this stage of the project, to be rather extensive over the entire surface and of significant thickness. Cold work done after the casting, and before the gilding, aimed to enhance the hair and beard details, using chisels, or cutting tools.
Since 1986, several conservation interventions have been carried out on the heads of Brescia. The portrait under examination, however, does not seem to have undergone restoration, except possibly for the light removal of some surface deposits, as can be inferred from a comparative analysis of historical images.
In this preliminary phase of study, prior to the restoration intervention, the first non-destructive scientific investigations were conducted using portable instruments and micro-sampling of surface material from both the external and internal surfaces. The 3D survey activities described in this paper were planned to support the restoration works from the Opificio delle Pietre Dure in Florence and had the measurement of the bronze thickness as primary objective. The main challenge in digitizing the head lies in measuring the inside surface passing through the narrow neck opening which spans ~ 8 cm in diameter.
The opportunity to conduct an interdisciplinary study of the head MR353 allows for a deeper understanding of the significance of this figurative program in relation to the history of ancient Brixia.

1.2 Paper objective

This paper presents the acquisition design choices made to digitize the MR353 roman bronze head using low-cost tools, with the goal of achieving full digitization of the artefact. We propose a straightforward and reliable solution for surveying the inner surface of the cast, employing an industrial-grade camera equipped with a fisheye lens mounted on a handheld pole, operated and controlled manually.
The proposed method is based on fisheye photogrammetry and utilizes a SfM pipeline. This approach seamlessly integrates the interior and exterior surveys into a unified SfM processing workflow. As a result, the entire artefact can be digitized using a single technique, producing a 3D model with consistent characteristics – such as accuracy, resolution, and material texture – on both the interior and exterior surfaces.
The paper also describes the results of analyses conducted on the 3D replica of the bronze head, which aimed to measure the thickness of the cast. This analysis was carried out using two distinct methods that produced consistent and overlapping results. Additionally, the paper discusses the creation of a 3D digital asset optimized for web dissemination, ensuring fruition to a broad audience.

2. Materials and Methods

The 3D survey was completed in a single day by one operator, with assistance during the setup and during the acquisition of the exterior surface. The activities took place on-site at the Santa Giulia Museum during a scheduled closure and were completed in approximately four hours. To ensure efficiency, all steps were pre-planned, and preliminary tests and preparations were carried out in advance. For instance, the custom camera probe used for the interior survey has been designed, assembled, and tested in advance. On site, the workflow was structured to first capture the exterior surface, followed by the interior surface, all within the same setup location. All movements of the bronze head were handled by specialized personnel to guarantee its safety. The following subchapters provide a detailed descriptions of the survey tools, methods and processing strategies.

2.1 Setup for the exterior surface survey

The exterior survey was conducted in a controlled environment using a high-resolution DSLR camera mounted on a tripod and the acquisition was carried out in a standard turntable setup. When standing upright, the artefact was secured at the centre of the turntable on the same stand used for its display in the museum. To address the issue of specular reflections, the cross-polarization technique, as described in Menna et al. (2016) and Mandelli et al. (2019), was implemented. This method requires all light sources illuminating the artefact to be polarized in the same direction (vertically, in our case), then, the light reflected by the artefact is filtered before entering the camera by using a circular polarizer mounted on the camera lens, rotated 90° with respect to the light polarization (horizontal in our case).
To exclude unpolarized ambient light, the setup was enclosed in a light-obscured environment, i.e., a blackout enclosure structure, assembled to fully envelope the artefact, operator, and illumination system. As shown in Figure 2, the enclosure was created using a dark cloth suspended on three light stands arranged in a triangular formation, with an additional dark cloth covering the top.
Lighting was provided by two flash lamps mounted on light stands and positioned approximately 1 m from the artefact. The lamps were aimed directly at the object with a converging angle to optimize illumination. A Nikon D810 DSLR, offering a resolution of 7360 × 4912 pixels, was used, equipped with the Nikon Micro 45mm f/2.8 tilt-and-shift lens. Although no tilt or shift adjustments were applied, the lens was selected for its optical quality and minimal focusing distance. The capturing distance was kept at approximately 65 cm, achieving a Ground Sampling Distance (GSD) of about 0.07 mm.
To create a comprehensive image network, the artefact was rotated on the turntable and the camera was set at few different heights. Flash lamps' positions were adjusted with the camera to keep aligned the light source with the camera's viewing direction. A total of 11 rotations were conducted: five complete turns with the artefact upright, three partial turns with the head lying on its right side, and three with the head on its left.
Images were captured every 10 gon of rotation, resulting in 40 images per complete turn and 20-25 images per partial turn (Figure 3, top). A total of 347 reflection-free images were captured with the cross-polarization setup. Additionally, 114 images were acquired every 40 gon of rotation without the cross-polarization setup, allowing for specular reflections (Figure 3, bottom). These datasets are referred to as Dataset EA (exterior – reflection-free) and Dataset EB (exterior – with reflections).

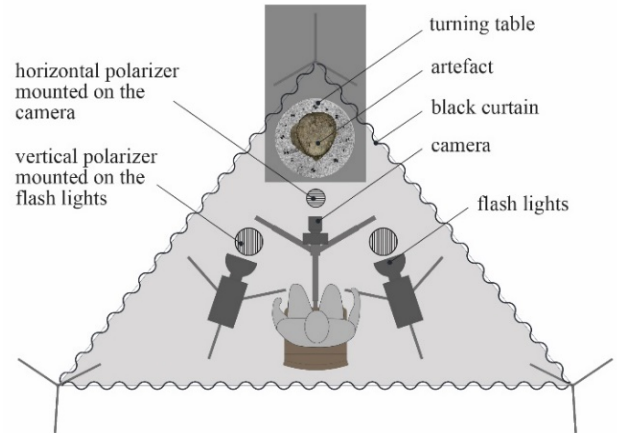

Figure 2. Scheme of the setup for the exterior surface acqusition.

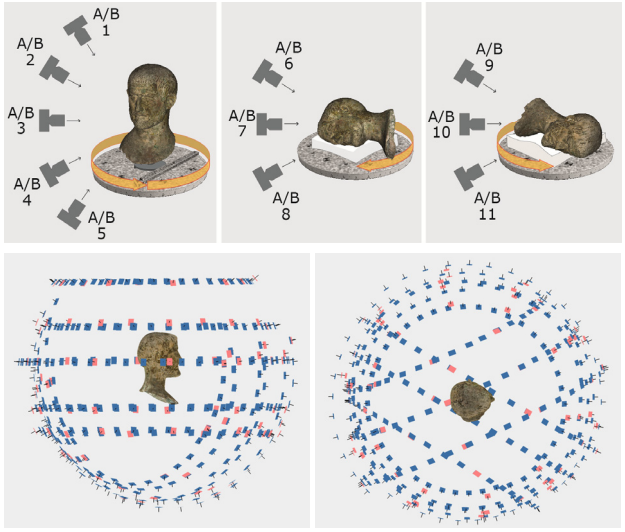

Figure 3. Scheme of the exterior image network: camera positions and artefact orientations (top), complete image network (bottom). For each configuration, images were acquired for dataset EA (reflection-free – blue) and dataset EB (with reflections – red).

Dataset EA provided the ideal input for accurate reconstruction and was used for the SfM processing to generate the artefact's 3D mesh model. Both datasets provided the image sets to generate two opposing material texture for the artefacts. Dataset EB enable the generation of a more realistic visual representation of the artefact's reflective properties, while Dataset EA enable the generation of a reflection-free texture map that reveals surface details obscured by reflections. Moreover, the reflection-free texture map, can be enhanced for rendering purposes by reintroducing specular properties as a material characteristic

Figures 4 compares images from the two datasets, the zoom in cuts highlights the surface details that are enhanced by the removal of reflections. Table 1 summarizes the main details about the performed acquisition.

Figure 4. Comparison between similar images from Dataset EA (left), and Dataset EB (right). zoomed in cuts on the bottom.

Datasets	# images	GSD	Purpose
Exterior (EA) reflection-free	347	0.07 mm	3D model Texture ype A
Exterior (EB) with reflections	114	0.07 mm	Texture type B
Interior (I)	966 (total) 681 *	0.13 mm**	3D model Texture

Table 1. Details about the different datasets.
(*) number of images used for 3D model processing, (**) GSD computed at the centre of the image frame.

2.2 Proposed method for the inside surface survey

For the survey of the interior surface, two different methods were initially considered: (1) a low-cost flexible endoscope able of capturing low-resolution images, and (2) a custom-assembled camera probe. Preliminary testing was conducted in the lab, and the endoscope method was discarded due to the poor image quality produced by the low-cost hardware. Additionally, the endoscope proved ineffective for framing the challenging chin undercut area. Consequently, we opted to assemble a custom camera probe that could be manually operated and adjusted to tilt the camera in various directions.

2.2.1 Selected hardware: The custom system consisted of the following components:

- Camera: A compact industrial RGB camera, FLIR Blackfly S 50S5, with a global shutter sensor featuring a resolution of 5 Megapixels (2448 × 2048).
- Lens: A compact fisheye lens, SUNEX DSL315 2.7mm f/2.3, offering a 190° field of view.

The camera was connected to a laptop via a single cable, which provided both power and triggering. Image capture was managed using the camera manufacturer's demo software, set to timed-capture mode.

2.2.2 Camera probe design: The camera and an illumination rig were mounted on a metal bar to create the camera probe. The design aimed to achieve two primary objectives:

- Compactness: The probe had to fit within the 8 cm diameter neck opening of the head, with sufficient clearance.
- Safety: The probe had to ensure no damage to the valuable artefact.

To meet these requirements, the probe head was designed with a footprint of 4 × 5 cm, and the metal bar was approximately 40 cm long. A smooth, semi-transparent plastic cover was wrapped around the camera and LED (light-emitting diode) lights to shield the artefact from any sharp edges. The bar was further covered with the same plastic material and a heat-shrinkable sheathing to ensure a completely smooth surface.
The illumination rig consisted of six loose LEDs temporarily fixed around the lens to form a compact ring light. These were powered by a portable power bank. Figure 5 illustrates the assembled camera probe with dimensions.

2.2.3 Acquisition workflow: During the survey, the head was positioned on its side, supported by Ethafoam, while the operator manually controlled the probe. The lens focus was pre-adjusted to approximately 10–15 cm. Five timed captures were conducted, with the camera viewing angle adjusted for each:

- **Capture 1**: The camera pointed forward, as shown in Figure 5 (see also Figure 6a and 6b).
- **Capture 2**: The camera was reversed, pointing back toward the operator (Figure 6c).
- **Capture 3**: The camera pointed forward and was tilted approximately 20° to the right around its anchor point to the bar.
- **Capture 4**: The camera was reversed and was tilted approximately 20° to the right around its anchor point to the bar (figure 6d).
- **Capture 5**: The camera again pointed forward, but the probe was manoeuvred around the neck opening to link the interior dataset with the exterior dataset.

For the first four captures, which focused on the interior surface, the probe was positioned at the neck opening before insertion. A circular motion was performed in front of the opening to image the wider area of the neck, serving as the connection point between the interior and exterior datasets. The probe was then inserted just past the narrowest part of the neck, where another circular motion was performed to capture as much of the interior surface as possible. This process was repeated multiple times across all captures to ensure a robust and redundant image

network. Captures 2 and 4 were crucial for framing all undercut areas of the interior (see Figure 6d).
A total of 966 images were acquired during the interior survey divided among the five captures. The GSD, computed at the centre of the image frame, considering an average capturing distance of 10 cm, is 0.13 mm (Table 1). Unlike the exterior survey, no cross-polarization technique was applied. However, due to the rough interior surface and absence of gilding, specular reflections were not observed. Figure 6 provides examples of the images captured with the proposed system, while Figure 7 show the complete image network.

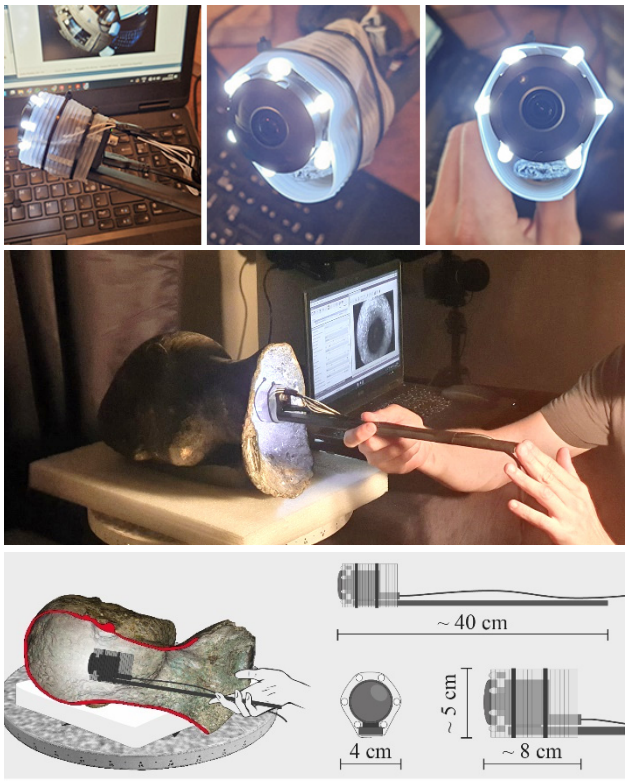

Figure 5. Images of the custom camera probe (top and centre), and scheme of the acquisition and dimensions (bottom).

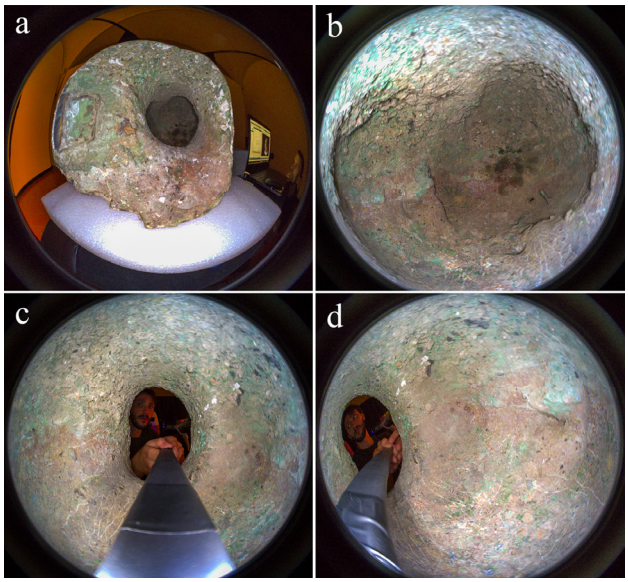

Figure 6. Image sample of the interior dataset: Capture 1, starting point of the acquisition (a), and inside the head (b); Capture 2 (c); Capture 4, framing the chin undercut (d).

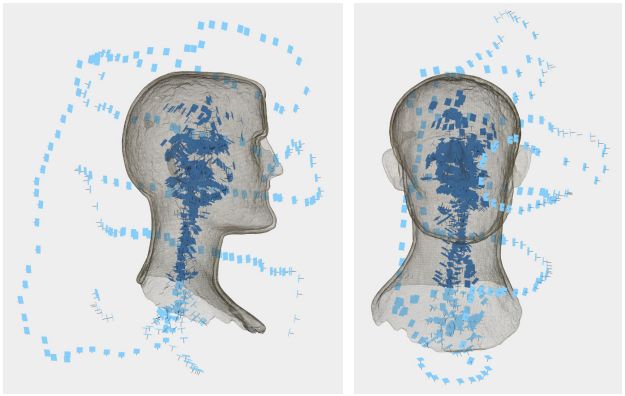

Figure 7. Image network of the interior surface survey showing all images acquired with the custom camera probe and used for the SfM. Only images in blue were used for processing the mesh model.

2.3 Processing and interior/exterior join

The processing steps are summarized in Figure 8. All images were pre-processed using a RAW-editing software to adjust brightness and colours, based on a colour profile calibration performed with the aid of a colour checker. Images from the exterior dataset were captured in RAW format, while those from the interior dataset were saved directly in JPG format. Despite this, the images acquired with the camera probe were pre-processed to match the exterior dataset in terms of colour balance and brightness (see Figure 6).
Photogrammetric processing was performed using Agisoft Metashape v2.1 (Agisoft inc. Development Team, 2024) to generate the final high-resolution 3D model of the bronze head. The workflow consisted of two main steps:

- **SfM of Dataset EA**: Images from Dataset EA, which were captured using cross-polarization and a comprehensive wrap-around image network, were processed first, as they were ideal for accurate 3D modelling. Background areas in the images were masked before the SfM processing.
  The resulting 3D model was scaled using known distances between markers on a calibrated aluminium reference bar (see Figure 1). The reference bar, calibrated with an accuracy of ±0.5 mm, was placed alongside the bronze head during the survey and shifted in three distinct locations as the head was repositioned.
- **Connecting Dataset EB and interior**: Once Dataset EA was aligned and scaled, images from Dataset EB and the interior dataset were aligned to it. During this step, the Exterior Orientation (EO) and Interior Orientation (IO) parameters of Dataset EA were fixed, while the EO and IO of the additional datasets were estimated.
  No direct control nor scaling measurements were possible for the interior dataset, as physical contact with the fragile artefact was to be avoided. Consequently, the accuracy of the entire reconstruction relied on the robust connection between the interior and exterior datasets. This connection was ensured by redundant imaging of the interior neck surface across all datasets. Additionally, Capture 5 from the camera probe dataset had the purpose of extending the link between the two datasets beyond the neck opening.

After aligning all datasets, the full-resolution mesh model was generated using images from Dataset EA and a subset of images from the interior dataset (those acquired exclusively inside the

head – see Figure 7, images in blue). No images from Dataset EB were used in the mesh processing.
The raw mesh model consisted of approximately 80M faces and underwent few geometric adjustments and refinements to ensure watertightness and resolve any non-manifold geometry issues.

2.4 Analysis and final products

From the resulting full-resolution 3D model, two separated processing have been initiated: on one hand the model was further processed to measure the thickness of the bronze head point to point; on the other hand, the model was processed to obtain an optimized digital asset for dissemination purposes.

2.4.1 Thickness analysis: The model thickness computation has been performed using two distinct approaches: the "ray method" and the "sphere method". As described by Inui et al. (2016), with the "ray method" the thickness of the model at a point ***p*** is given by the Euclidean distance between the point ***p*** and the opposite surface along the local normal ray; with the "sphere method", instead, the thickness of the model at a point ***p*** is given by the diameter of the maximum inscribed sphere within the model, touching ***p***. In order to compute the cast's thickness with the two approaches, we relied on the following algorithms: (1) The M3C2 algorithm (Laque et al., 2013), available as a plug in of CloudCompare v2.13 (CloudCompare Development Team, 2024); and (2), the Shrinking sphere algorithm (Inui et al., 2016), available in the MeshLib python module (MeshLib Development Team, 2024). For both approaches, the input data was a decimated version of the 3D model, sampled down to a resolution of ~10M faces.

- **M3C2 algorithm**: To compute the thickness with this method, the mesh model was downsampled to a point cloud and the interior and exterior surfaces were separated by segmenting the head around the neck boundary. The outer surface was used to compute the normals, and the thickness measurement was taken as the absolute value of the M3C2 distance between the two point clouds along the normal directions.
- **Shrinking Sphere algorithm**: With this method the thickness is computed directly on the mesh, point by point using its vertexes. We returned a point cloud as the output, composed of the mesh vertexes associated with a scalar field representing the resulted thickness.

2.4.2 Optimized digital asset: The digital asset was obtained by remeshing the source 3D model to a low-poly version and by encoding the lost geometric details as 2D material maps, e.g., diffuse map, occlusions map and normal map (Verhoeven, 2017; Apollonio et al., 2021). The step followed are the same described in Perfetti et al. (2022), i.e.:

- **Model(s) preparation**: from the full resolution 3D model, two decimated versions have been derived: (1) a high-poly model preserving all relevant geometric details; and (2) a low-poly versions preserving object shape only.
- **Retopology**: A simplified quadrangular mesh was derived by remeshing the low-poly model.
- **UV unwrapping**: the quadrangular mesh model was used to manually define the UV parametrization of the model.
- **Details recovery**: Geometric details are re-introduced to the low-poly model from the high-poly model by faces subdivision and vertexes adjustments until the desired geometric simplification is reached.
- **Texture backing**: The diffuse, occlusion and normal material maps are computed for the low-poly model using the high-poly as reference. At this stage two diffuse maps are generated for the low-poly model, a Type A using, from the exterior datasets, only images from Dataset EA, and a Type B using those from Dataset EB (Figure 8)

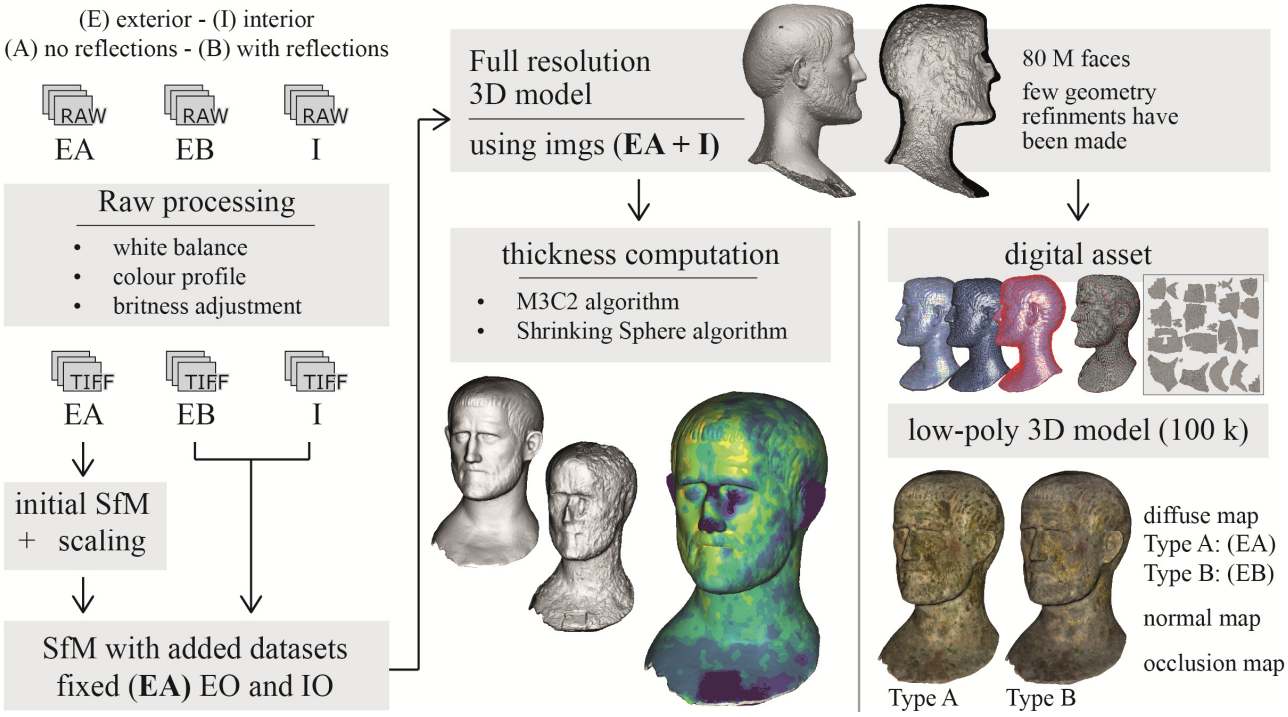

Figure 8. Outline of the processing pipeline.

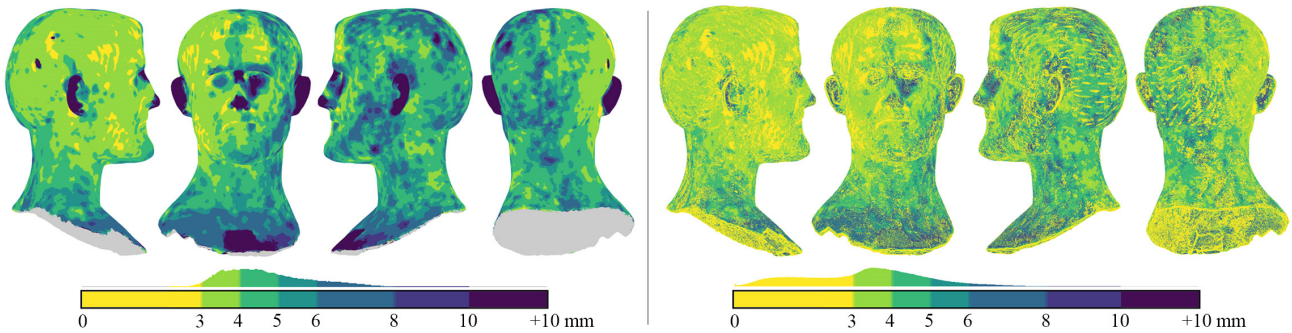

Figure 9. Result of the cast's thickness measurements employing the two methods: “ray method” using the M3C2 algorithm (right), and “sphere method” using the Shrinking Sphere algorithm (left).

3. Results

3.1 Thickness measurement

The results of the thickness measurements are shown in Figure 9. The right side presents the measurements obtained using the “ray method” employing the M3C2 algorithm, while the left side illustrates those derived from the “sphere method” employing the Shrinking Sphere algorithm.

Although the plots appear different at first – particularly because the sphere method return numerous points with a thickness of less than 3 mm (indicated in yellow) – the overall results are highly similar and largely overlap. The low thickness values reported by the sphere method arise due to the rough surface of the cast, which is characterized by irregularities and small protruding features. In these protruding areas, the maximum inscribed sphere is relatively small, leading to the observed low thickness readings. However, since the primary focus of the analysis is the general thickness of the bronze cast, these outliers should be filtered out.

The ray method provides clearer and more interpretable results because the local normals of the outer surface are estimated using a neighbouring radius such to exclude small surface irregularities. Nevertheless, the M3C2 method does not generate thickness values for certain regions, such as the inner surface (depicted in grey on the right-side plots) and the ears. The ears are shown with a high thickness value exceeding 10 mm, obtained by extending the thickness readings at the boundary of the ear geometry to the whole ear. The actual thickness measurements of the ears, as defined in the ray method, cannot be computed, as rays cast along the normal direction from the ear tips do not intersect the inner reference surface. Conversely, the sphere method provides thickness estimates for both the ears and the inner surface. However, the inner surface's roughness leads to numerous low thickness values when using this method.

A comparison of the two methods, after excluding the low thickness readings from the sphere method (< 3mm) caused by surface irregularities, yields consistent results. The minimum measured thickness of the bronze cast is approximately 2.8 mm.

3.2 Digital asset

The optimized 3D model is a low-poly version with a resolution of 100,000 faces. Despite its reduced geometry, the model effectively preserves the details of the high-resolution version during rendered visualizations, thanks to the computed high-resolution texture maps. Each texture map was generated at 8K resolution. Figure 10 presents the rendered low-poly model, while Figure 11 offers zoomed-in views of the digital asset, demonstrating how the texture maps enhance the representation.

Figure 10. Renders of the low-poly 3D model, from image dataset A (right) and image dataset B (left).

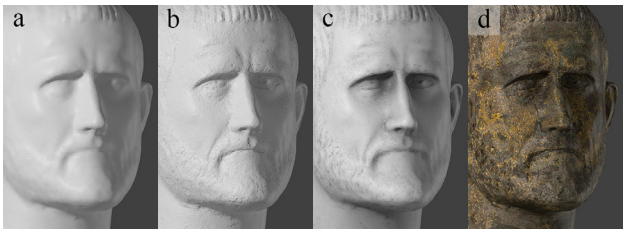

Figure 11. Low-poly 3D asset (a) with material maps applied: normal map (b), occlusion map (c), all maps (d).

4. Conclusions

As a result of the photogrammetric digitization, a comprehensive 3D model of the artefact has been created. The high-resolution model (Figure 1) consists of 80 M faces, while the optimized digital asset has been reduced to 100,000 faces.

The full digitization was achieved employing solely close-range photogrammetry, by developing ad-hoc solutions utilizing low-cost hardware. The proposed solution enabled the accurate capture of both the geometric structure and material textures of the interior surface of a bronze head through a custom-assembled camera probe. The system proved cost-effective, with the camera probe's hardware costing less than €1,000. Additionally, the proposed method, by employing a single acquisition technique, offer a simple and straightforward processing workflow. Future work could focus on enhancing the camera probe system by upgrading the ring light and incorporating polarizing filters, allowing cross-polarization techniques to be extended to interior surface surveys as well.

Acknowledgements

The authors would like to express their gratitude to the staff of the Museo di Santa Giulia in Brescia for their support throughout the project. Special thanks are extended to Gexcel S.r.l., particularly Dr. Massimo Gelmini, for their contributions to the planning and preparation stages, as well as for their assistance during the survey activities.

References

Adami, A., Fregonese, L., Helder, J., Rosignoli, O., Taffurelli, L., Treccani, D., 2022: High-resolution digital survey of floors: a new prototype for efficient photogrammetric acquisition. *Int. Arch. Photogramm. Remote Sens. Spatial Inf. Sci.*, XLIII-B2-2022, 745–752.

Agisoft inc. Development Team, 2024. Agisoft Metashape v2.1 Software, url: https://www.agisoft.com/ (last accessed: November 2024).

Albertin, F., Bettuzzi, M., Brancaccio, R., Morigi, M. P., Casali, F., 2019: X-Ray computed tomography in situ: an opportunity for museums and restoration laboratories. *Heritage 2*, 2028–2038.

Apollonio, F.I., Fantini, F., Garagnani, S., Gaiani, M., 2021: A photogrammetry-based workflow for the accurate 3D construction and visualization of museums assets. *Remote Sensing*, 13, 486.

Artec3D inc., 2024. Portable 3D scanners, url: https://www.artec3d.com/portable-3d-scanners (last accessed: November 2024).

Bettuzzi, M., Casali, F., Morigi, M. P., Brancaccio, R., Carson, D., Chiari, G., Maish, J., 2015: Computed tomography of a medium size Roman bronze statue of Cupid. *Appl. Phys. A 118*, 1161–1169.

Bici, M., Gherardini, F., Campana, F., Leali, F., 2020: A preliminary approach on point cloud reconstruction of bronze statues through oriented photogrammetry: the "Principe Ellenistico" case. *IOP Conf. Ser.: Mater. Sci. Eng*. 949, 012117.

Bossema, F. G., Palenstijn, W. J., Heginbotham, […], 2024: Enabling 3D CT-scanning of cultural heritage objects using only in-house 2D X-ray equipment in museums. *Nat Commun 15*, 3939.

Brini, A., Morandini, F., Patera, A., Pucci, E., (in press): I ritratti virili in bronzo di Brescia. Studi preliminari sulla doratura. *In: Patera A., Vernillo A., "Dal frammento all'intero: i bronzi dei Renai di Signa. Restauri e indagini sulla statuaria antica in bronzo dorato"*.

CloudCompare Development Team, 2024. CloudCompare v2.13 Software, url: https://www.cloudcompare.org/ (last accessed: November 2024).

Comte, F., Pamart, A., Réby, K., De Luca, L., 2024: Strategies and experiments for massive 3D digitalization of the remains after the notre dame de paris' fire. *Int. Arch. Photogramm. Remote Sens. Spatial Inf. Sci.*, XLVIII-2-W4-2024, 127–134.

Creaform inc., 2024. Professional and Industrial Portable 3D Scanners, url: https://www.creaform3d.com/en/portable-3d-scanners (last accessed: November 2024).

Guidi, G., Micoli, L. L., Gonizzi, S., Brennan, M., Frischer, B., 2015: Image-based 3D capture of cultural heritage artefacts an experimental study about 3D data quality. *Digital Heritage*. 321–324.

Hallot, P., Gil, M., 2019: Methodology for 3D acquisition of highly reflective goldsmithing artefacts. *Int. Arch. Photogramm. Remote Sens. Spatial Inf. Sci.*, XLII-2-W17, 129–134.

Inui, M., Umezu, N., Shimane, R., 2016: Shrinking sphere: a parallel algorithm for computing the thickness of 3D objects. *Computer-Aided Design and Applications*, 13, 199–207.

Kalinowski, P., Füldner, K., Mittmann, M., Schierbaum, A., Luhmann, T., 2022: High accuracy 3D digitisation of the goethe elephant skull using hand-held 3D scanning systems and structure from motion – a comparative case study. *Int. Arch. Photogramm. Remote Sens. Spatial Inf. Sci.*, XLVI-2-W1-2022, 275–281.

Lague, D., Brodu, N., Leroux, J., 2013: Accurate 3D comparison of complex topography with terrestrial laser scanner: Application to the Rangitikei canyon (N-Z). *ISPRS Journal of Photogrammetry and Remote Sensing*, 82, 10–26.

Lauria, G., Sineo, L., Ficarra, S., 2022: A detailed method for creating digital 3D models of human crania: an example of close-range photogrammetry based on the use of Structure-from-Motion (SfM) in virtual anthropology. *Archaeol Anthropol Sci 14*, 42.

Mandelli, A., Perfetti, L., Fiorillo, F., Fassi, F., Rossi, C., Greco, C., 2019: The digitalization of ancient egyptian coffins: a discussion over different techniques for recording fine details. *Int. Arch. Photogramm. Remote Sens. Spatial Inf. Sci.*, XLII-2-W15, 743–750.

Marshall, M. E., Johnson, A. A., Summerskill, S. J., Baird, Q., Esteban, E., 2019: automating photogrammetry for the 3D digitisation of small artefact collections. *Int. Arch. Photogramm. Remote Sens. Spatial Inf. Sci.*, XLII-2-W15, 751–757.

Menna, F., Nocerino, E., Remondino, F., Dellepiane, M., Callieri, M., Scopigno, R., 2016: 3D digitization of an heritage masterpiece – a critical analysis on quality assessment. *Int. Arch. Photogramm. Remote Sens. Spatial Inf. Sci.*, XLI-B5, 675–683.

Menna, F., Nocerino, E., Morabito, D., Farella, E. M., Perini, M., Remondino, F., 2017: An open source low-cost automatic system for image-based 3D digitization. *Int. Arch. Photogramm. Remote Sens. Spatial Inf. Sci.*, XLII-2-W8, 155–162.

MeshLib Development Team, 2024. MeshLib Python modul, url: https://github.com/MeshInspector/MeshLib/ (last accessed: November 2024).

Nicolae, C., Nocerino, E., Menna, F., Remondino, F., 2014: Photogrammetry applied to Problematic artefacts. *Int. Arch. Photogramm. Remote Sens. Spatial Inf. Sci.*, XL–5, 451–456.

Patera A., Morandini F., 2021: *Necessitano alla Vittoria Alata le cure del restauratore. Studi, indagini e restauro del grande bronzo di Brescia*. Edifir, Firenze.

Perfetti, L., Teruggi, S., Achille, C., Fassi, F., 2022: Rapid and low-cost photogrammetric survey of hazardous sites, from measurements to VR dissemination. *Int. Arch. Photogramm. Remote Sens. Spatial Inf. Sci.*, XLVIII-2-W1, 207–214.

Santos, P., Ritz, M., Tausch, R., […], 2014: CultLab3D – on the verge of 3D mass digitization. *The Eurographics Association*, 9.

Santos, P., Ritz, M., Fuhrmann, C., Fellner, D., 2017: 3D mass digitization: a milestone for archeological documentation. *Virtual Archaeology Review,* 8, 1–11.

Verhoeven, G.J., 2017: Computer graphics meets image fusion: the power of texture baking to simultaneously visualise 3D surface features and colour. *ISPRS Annals of Photogramm. Remote Sens. Spatial Inf. Sci.*, IV-2/W2, 295-302.

Wells, J., Jones, T., Danehy, P., 2005: Polarization and colour filtering applied to enhance photogrammetric measurements of reflective surfaces. *46th AIAA/ASME/ASCE/AHS/ASC Structures, Structural Dynamics and Materials Conference*.